Materials Today Bio 28 (2024) 101170

Contents lists available at ScienceDirect

Materials Today Bio

journal homepage: www.journals.elsevier.com/materials-today-bio

Unveiling the governing role of 'remodeling triangle area' in soft-hard tissue interface equilibrium for metal implants advancement

Shoucheng Chen [a,1], Guangqi Gao [a,1], Jiamin Shi [a,1], Na Li [a,1], Lv Xie [a], Yingye Zhang [a], Zhengjie Shan [a], Jiaxin Xie [a], Yin Xiao [b,***], Zhuofan Chen [a,**], Zetao Chen [a,*]

[a] Hospital of Stomatology, Guanghua School of Stomatology, Sun Yat-sen University and Guangdong Research Center for Dental and Cranial Rehabilitation and Material Engineering, Guangzhou, 510055, China

[b] School of Medicine and Dentistry, Griffith University (GU), Gold Coast, QLD, 4222, Australia

ARTICLE INFO

Keywords:
Metal implant
Dental implants
Soft-hard tissue interface equilibrium
Remodeling triangle area
Immune modulation

ABSTRACT

Metal implants holds significant promise for diverse fixed prostheses. However, their long-term reliability and broader application are hindered by challenges related to the disequilibrium at the soft-hard tissue interface. By using anti-inflammatory (PDA/IL4) and pro-inflammatory (PDA/LPS/IFNγ) coatings to modulate distinct immune characteristics, we discovered a dynamic bioactive structure at the soft-hard tissue interface around metal implant, which we have named the 'Remodeling Triangle Area' (RTA). We further demonstrate that the RTA can be influenced by the PDA/IL4 coating to favor a phenotype that enhances both innate and adaptive immunity. This leads to stronger epithelial adhesion, the formation of dense connective tissue via IGF1 secretion, and a more balanced soft-hard tissue interface through the OPG/RANKL axis. Conversely, the PDA/LPS/IFNγ coating shifts the RTA towards a phenotype that activates the innate immune response. This results in a less cohesive tissue structure and bone resorption, characterized by reduced IGF1 secretion and an imbalanced OPG/RANKL axis. Over all, our study introduces the novel concept termed the 'Remodeling Triangle Area' (RTA), an immune-rich anatomical region located at the nexus of the implant interface, epithelial, connective, and bone tissue, which becomes highly interactive post-implantation to modulate the soft-hard tissue interface equilibrium. We believe that an RTA-centric, immunomodulatory approach has the potential to revolutionize the design of next-generation metal implants, providing unparalleled soft-hard tissue interface equilibrium properties.

1. Introduction

Metal implants, renowned for their exceptional mechanical properties, are increasingly employed in the fixation of prostheses such as oral implants, prosthetic limbs, eyes, noses, and ears in medical applications [1,2]. Simultaneously, due to their ability to provide stable and direct transcutaneous communication, these implants possess substantial potential in fields like advanced osseointegrated prosthetics (Fig. 1A) [3]. As a material that collaborates with both soft and hard tissues, the long-term success of metal implants hinges critically on the effective management of the surrounding soft and hard tissues [4,5]. There have been many studies exploring soft tissue-implant or bone-implant integration, respectively, such as physical modification (roughness, topology, *etc.*), chemical modification (plasma polymerization, *etc.*), and bioactive factors (ion implantation, *etc.*) [6–8]. Similarly, there are currently increasing studies on surface modification of zirconia materials to promote better soft tissue integration [9]. These efforts have achieved partial success in managing individual implant-tissue interfaces [10,11]. However, challenges remain, especially at the dynamic equilibrium of the soft-hard tissue interface, where some degree of imbalance has historically been inevitable [12,13]. For instance, implants often suffer rapid bone loss of 1–1.5 mm post-implantation. Soft tissue encroachment poses further risks, particularly in acute inflammatory situations, leading to potential rapid implant failure due to significant bone loss (Fig. 1B) [14,15].

Furthermore, the behavior of soft tissues, such as epithelial and

* Corresponding author.
** Corresponding author.
*** Corresponding author.
E-mail addresses: yin.xiao@griffith.edu.au (Y. Xiao), chzhuof@mail.sysu.edu.cn (Z. Chen), chenzet3@mail.sysu.edu.cn (Z. Chen).
[1] These authors contributed equally to this work.

https://doi.org/10.1016/j.mtbio.2024.101170
Received 17 May 2024; Received in revised form 13 July 2024; Accepted 27 July 2024
Available online 31 July 2024

fibrous tissues, significantly impacts hard tissue behavior. For example, *in vitro* experiments show that epithelial and fibroblast cells can directly regulate osteoblast and osteoclast activities. Epithelial cells are known to promote osteoclastogenesis through the protein kinase A signaling pathway [16]. Stimulated by lipopolysaccharides (LPS), human gingival fibroblasts can inhibit the differentiation of monocytes into bone-resorbing osteoclasts, mediated by osteoprotegerin (OPG) production [17]. Research has also identified the potential of fibroblast cells to directly transform into osteoblasts, thereby mediating bone regeneration [18]. The effective healing and robust integration of epithelial and connective tissues with metal implants emerge as critical factors not only for the immediate success of the implantation but also for the long-term stability and health of the adjacent hard tissues [19]. This integration acts as a protective barrier against external stimuli, significantly reducing the risk of inflammation and further promoting hard tissue repair and regeneration, as demonstrated by the lactoferrin-derived amyloid coating [20]. These observations underscore the necessity of viewing peri-metal implant soft and hard tissues as an interconnected complex, governing their equilibrium as a whole.

A comprehensive understanding of the soft-hard tissue interface equilibrium is pivotal for the advancement of metal implants. The intricate dynamic interactions at this interface, encompassing epithelium, fibroblasts, inflammatory cells, osteoblasts, and osteoclasts, pose significant challenges [21]. In the critical process of metal implantation, which involves incising and lifting soft tissues before preparing the osseous cavities, a distinct, trauma-induced separation at the interface between soft and hard tissues around the implant invariably occurs [22,23]. This separation may form a crucial zone, strategically located along the implant interface, adjacent to connective tissue and peri-implant bone tissue. In light of this, we hypothesize the existence of an undefined remodeling zone around metal implants, which is crucial for governing the equilibrium and forming a new interface between soft and hard tissues (Fig. 1C).

During the formation of the proposed anatomical structure, the immune microenvironment post-implantation demands attention. The rapid mobilization of immune cells to implant sites positions them as early cellular responders, influencing initial tissue responses and subsequent healing processes [24]. Their influence extends to regulating neighboring soft and hard tissue cells. For instance, immune cells can secrete cytokines and growth factors such as insulin-like growth factor-1 (IGF1), platelet-derived growth factor (PDGF), and C–C motif chemokine 22 (CCL22), crucial for fibroblast proliferation and extracellular matrix synthesis and remodeling [25]. The balance they maintain by secreting both receptor activator of NF-kB ligand (RANKL) and osteoprotegerin (OPG) is essential in governing osteoclast differentiation and function via the RANKL/OPG axis [26–28]. The remarkable regulatory potential of the immune response, depending on the stimuli, can induce different immune microenvironments, providing opportunities for

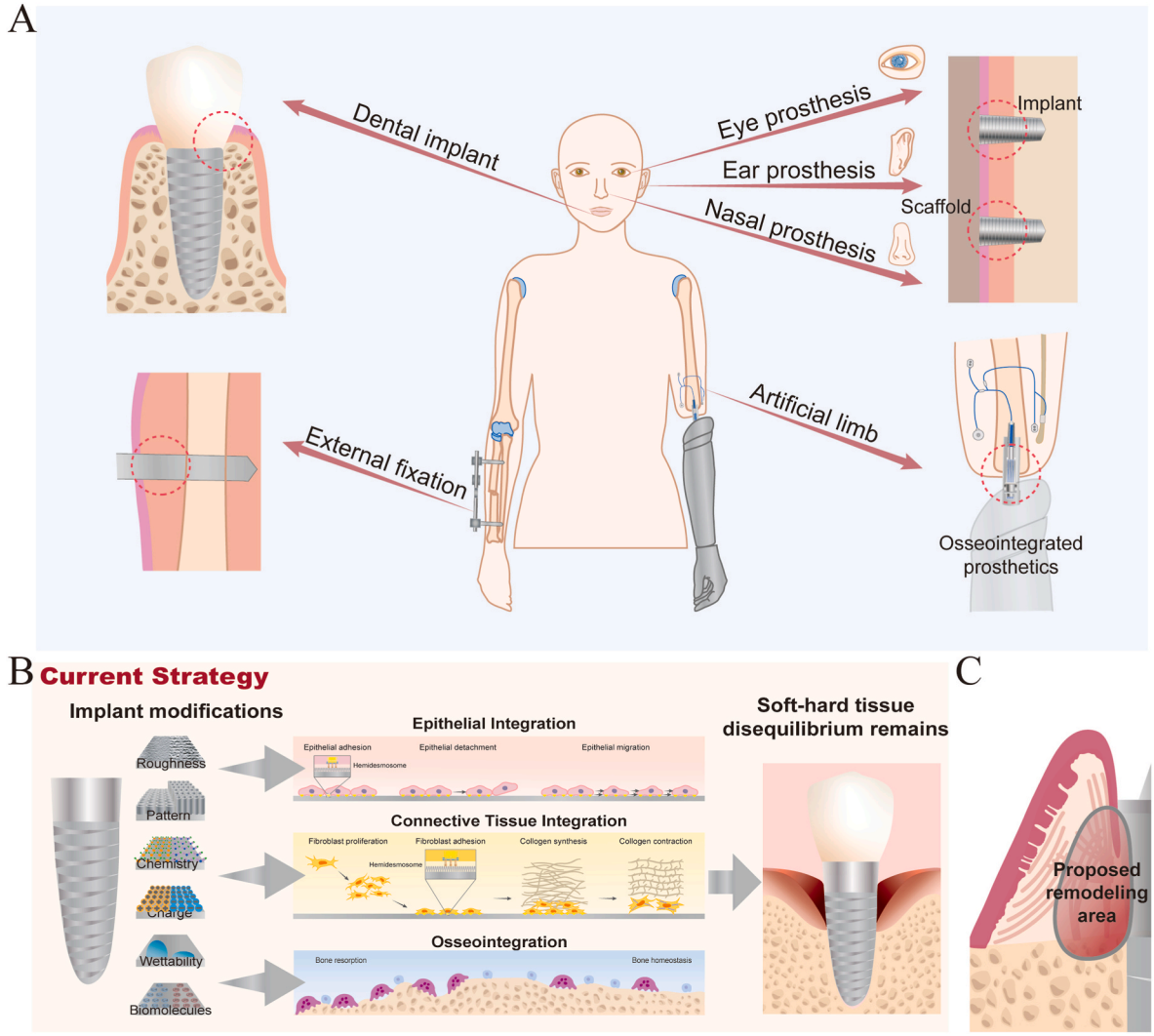

Fig. 1. Research background and experimental design. A) The high clinical demands for metal implants and their promising application. B) Strategies for improving implant-soft and -hard tissue integration individually. C) The potential anatomical remodeling area around the metal implant are undefined and understudied.

intervention [23,29]. Regulating the immune microenvironment may allow intervention in the complex balance at the soft-hard tissue interface around the implant and reveal the nature of this anatomical remodeling structure.

Our research aims to identify the proposed dynamic remodeling structure by modulating the peri-implant towards distinguished immune characteristics employing immune-modulatory coatings (PDA/IL4 and PDA/LPS/IFNγ). Each of these coatings plays a distinct role, with IL4 known for activating adaptive immune responses and exerting anti-inflammatory effects. At the same time, LPS/IFNγ are typically

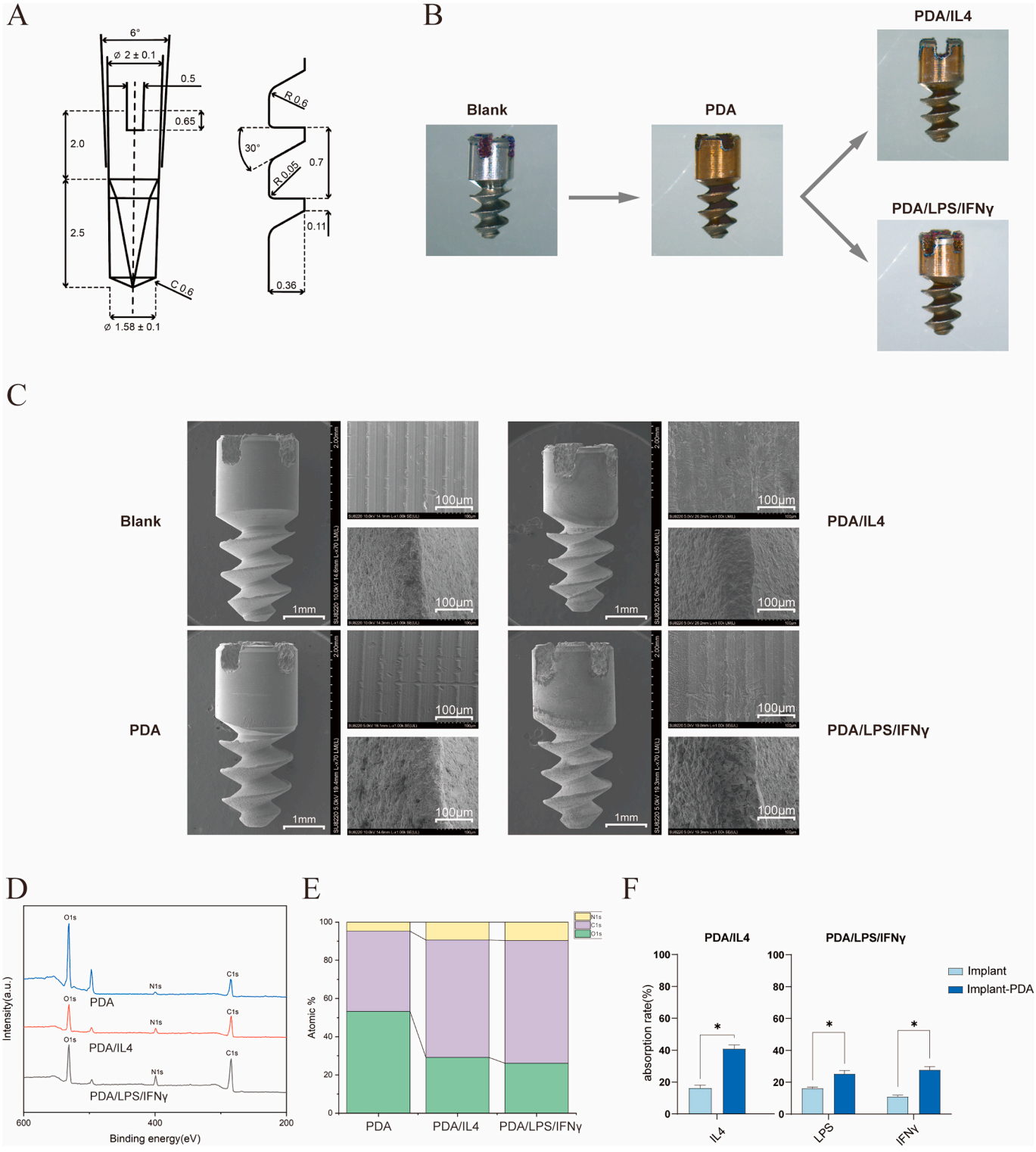

Fig. 2. Preparation of normal, pro-inflammatory, and anti-inflammatory metal implants. A) The design of the mini metal implants. The left segment delineates the general dimensions and geometric attributes of the implant, The right segment is dedicated to showcasing the thread details. B) An overview of the modification (PDA, PDA/LPS/IFNγ, and PDA/IL4 coatings) used in this study. C) SEM images of mini-metal implants, with PDA coating, PDA/IL4 coating, and PDA/LPS/IFNγ coating. D) XPS spectra of the mini implants before and after PDA, LPS/IFNγ and IL4 coatings. The PDA, PDA/LPS/IFNγ and PDA/IL4 groups showed an N1s peak (399.9 eV). E) N1s element content rose after LPS/IFNγ and IL4 coatings. F) Adsorption rates of LPS, IFNγ and IL4 evaluated by ELISA assay. $*p < 0.05$.

associated with pro-inflammatory effects. Further transcriptome sequencing and proteome spatial partitioning analysis were utilized to dissect the effect and mechanism of the proposed dynamic remodeling structure in regulating soft-hard tissue interface equilibrium around metal implants. This exploration is not just about enhancing our theoretical understanding; it is aimed at yielding practical, applicable strategies for governing the vital soft-hard tissue interface equilibrium property in next-generation metal implants.

2. Results and discussions

2.1. Preparation of modified metal implants

Specialized coatings on mini-metal implants were synthesized to decipher the interactions between metal implants and peri-implant soft-hard tissue interface equilibrium. The intricate design of these mini-implants is delineated in Fig. 2A, with the implant threads measuring 2.5 mm in length and the transgingival components extending 2 mm in both length and diameter. These coatings, consisting of a PDA base, were tailored to carry either anti-inflammatory or pro-inflammatory agents (IL4 and LPS/IFNγ respectively). IL4 and IFNγ are cytokines that have immunomodulatory and macrophage polarization effects, but they are challenging to adhere to biologically inert materials [30]. PDA is a biomimetic adhesive coating that can integrate into various biomaterial interfaces and form covalent bonds with biomolecules, making it a suitable substrate for bio-coatings.

The effective deposition of the PDA layer, in concert with LPS/IFNγ and IL4 on the mini-implants, was initially evidenced by a visual color

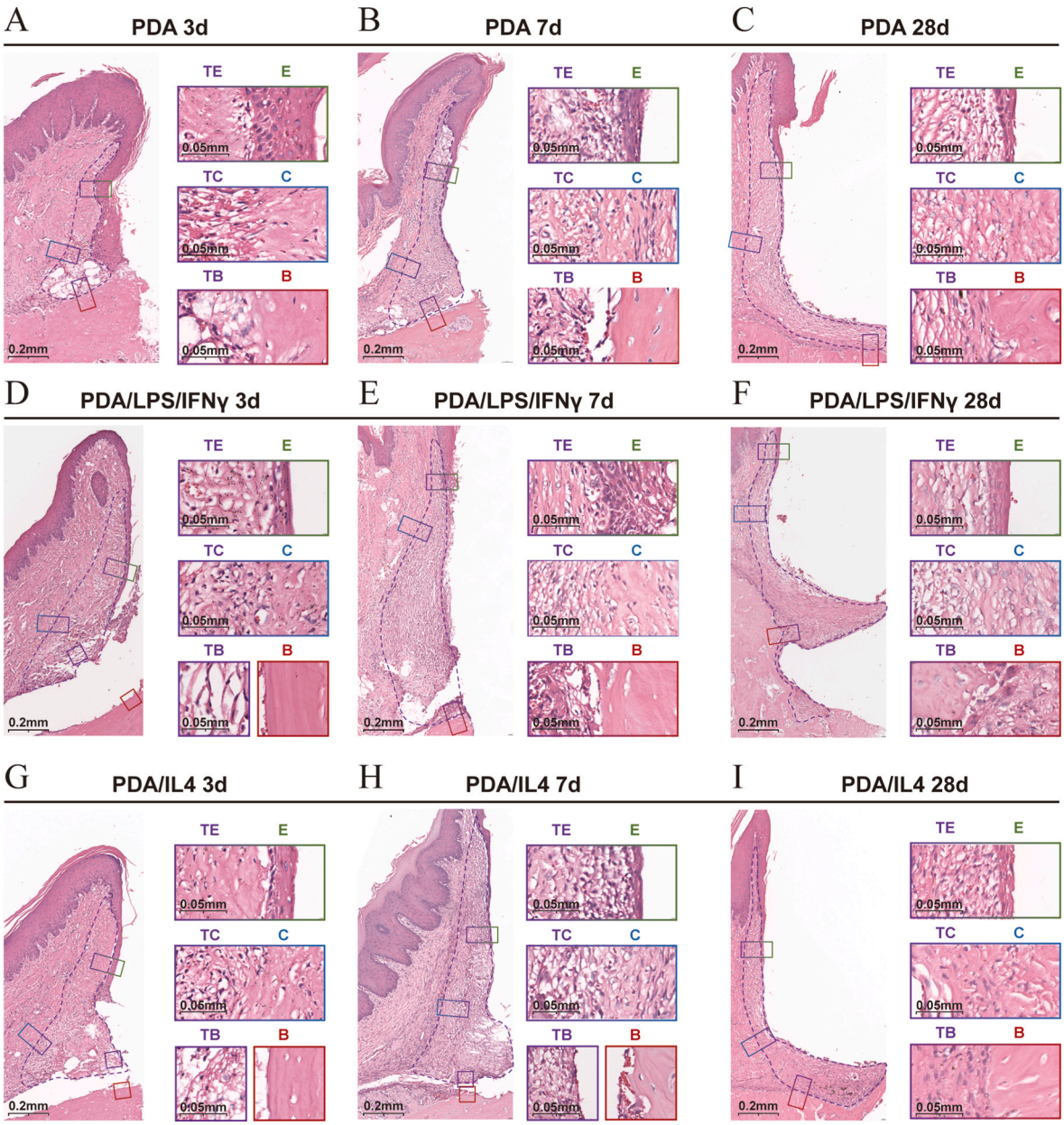

Fig. 3. The soft-hard tissue dynamics alterations around metal implants of three groups post-implantation. A-C) Typical H&E staining images presenting the dynamic changes of the remodeling triangle area (RTA) and surrounding tissues in the PDA group at day 3 (A), 7 (B), and 28 (C). D-F) The dynamic changes of the RTA and surrounding tissues in the PDA/LPS/IFNγ group at day 3 (D), 7 (E), and 28 (F). G-I) The dynamic changes of the RTA and surrounding tissues in the PDA/IL4 group at day 3 (G), 7 (H), and 28 (I). Rectangles on the right of each figure are magnified presentations of three interfaces (RTA-epithelium, RTA-connective tissue, and RTA-bone). TE, triangle-epithelium segment; E, epithelium; TC, triangle-connective tissue segment; C, connective tissue; TB, triangle-bone segment; B, bone.

transition, as illustrated in Fig. 2B. This preliminary indication was substantiated by detailed analyses using Scanning Electron Microscopy (SEM) and X-ray Photoelectron Spectroscopy (XPS), which confirmed the coating's presence and composition. SEM images showed that the PDA-coated surface had granular attachments, which were absent in the blank group, indicating the presence of a coating (Fig. 2C). The PDA/IL4 and PDA/LPS/IFNγ groups had rougher surfaces under SEM. The detection of the N1s peak (399.9 eV) on the surface further confirmed that there was an organic substance containing elemental N attached (Fig. 2D). The introduction of IFNγ and IL4 in the coating increased the N1s content of the coating compared to the PDA group, indicating the presence of amino and peptide bonds. The N1s element content rose from 4.1 % in the PDA group to 9.3 % and 8.8 % in the IFNγ and IL4 groups, respectively (Fig. 2E). Complementary to these findings, Enzyme-Linked Immunosorbent Assay (ELISA) results demonstrated a marked reduction of LPS, IFNγ, and IL4 levels in the surrounding medium, which paralleled an observed increase in their adsorption onto the implant surfaces (Fig. 2F). These consistent observations support the successful immobilization of PDA and cytokines on the implants, underpinning their prospective role in modulating the immune microenvironment adjacent to metal implants. Including a PDA-coated control allowed us to isolate the cytokines' specific contributions to the RTA, facilitating a clear distinction between cytokine modulation and PDA's baseline characteristics. While adding a non-coated control could provide a more comprehensive understanding, this study did not include a non-coated control as it is an initial exploration of the RTA and adheres to the 3R principles. Building upon this, we intend to assess further the *in vivo* soft-hard tissue interface equilibrium performance of these micro-metal implants in a delayed implantation animal model involving the maxillary first molar of rats (Fig. S1).

2.2. The soft-hard tissue dynamics alterations of the PDA group

To explore the pathophysiological changes of soft tissue interface following the implantation of metal implants, we initially observed the balance between soft and hard tissues around polydopamine-coated (PDA) implants at 3-, 7- and 28-days post-implantation (Fig. 3A–C).

2.2.1. 3 Days post-implantation

Three days after implantation, significant epithelial tissue migration towards the bone interface was observed, accompanied by noticeable thickening - a natural response to trauma. The bone tissue preserved its histological integrity, indicating robust osteogenic resilience. A distinctive 'remodeling triangle area' (RTA) formed in the peri-implant connective tissue, demarcated by neo-epithelium, unchanged connective tissue, and intact bone. This area presented a layered, highly interactive histological structure. In the Triangle-Epithelium Segment (TE), collagen fibers underwent hydropic degeneration, with fibroblast infiltration and necrosis near the epithelial basement membrane. The middle Triangle-Connective Tissue Segment (TC) displayed blood clots, intense collagen connective remodeling, and extensive cell infiltration. Finally, the Triangle-Bone Segment (TB) was characterized by an infiltrative loose network of blood clots and immune cells, with collagen fibers extending deep into the bone interface (Fig. 3A).

2.2.2. 7 Days post-implantation

By the seventh day, there was a notable shift towards a new equilibrium at the soft-hard tissue interface. The epithelial tissue began to return to its original position, thinning as it redefined its boundary with the implant surface. The RTA continued to exhibit a more uniform fibrous reconstruction and increased immune cell infiltration, indicating significant immune remodeling. Inflammation, reconstruction, proliferation, apoptosis, and a loose collagen network characterized the TE, TC, and TB segments. Notably, inflammatory fibrous complexes closely adhered to the basal membrane in the TE area and to the unchanged connective tissue in the TC area. The TB area evolved from a loose coagulation network to a highly ordered collagen matrix network, showing intense interactivity with the bone tissue (Fig. 3B).

2.2.3. 28 Days post-implantation

By day 28, a preliminary equilibrium was established between the soft and hard tissue interfaces. The junctional epithelium stabilized, aligning with increased bone density at the implant thread. The RTA showed reduced inflammation and a more structured collagen network. Specifically, the TE area still exhibited a relatively loose collagen structure with extensive fibroblast infiltration, though the epithelium was mature with a continuous basal membrane (Fig. S4). The TC area displayed mature collagen fibers with a decrease in immune cells, replaced by fibroblasts, and a reduced density of undifferentiated fibroblasts. In the TB area, the reconstructed collagen connective tissue became highly ordered and parallel to the implant interface, with immune cells being replaced by fibroblasts. At this stage, the interface fibrous tissue and bone surface adhered closely, forming a dense and smooth bone interface indicative of a balanced soft-hard tissue interface (Fig. 3C).

2.3. The soft-hard tissue dynamics alterations of the PDA/LPS/IFNγ group

Following the PDA group, we continued to examine the changes in the soft-hard tissue interface balance around metal implants with pro-inflammatory coating modifications at 3-, 7-, and 28 days post-implantation (Fig. 3D–F).

2.3.1. 3 Days post-implantation

At this stage, epithelial tissue in the PDA/LPS/IFNγ group also descended towards the bone interface but, unlike the PDA group, did not show significant epithelial thickening. A thick, dense layer formation was observed around the bone-implant interface. In the peri-implant connective tissue, a similar 'remodeling triangle area' (RTA) was noted, demarcated by neo-epithelium, unremodeled connective tissue, and intact bone. This group's RTA exhibited differentiated layered remodeling and heightened soft-hard tissue interaction. In the TE segment, there was pronounced connective tissue remodeling, marked by edematous changes and increased cellular infiltration, tightly adhering to the epithelium with an absence of a typical epithelial basement membrane. The TC segment primarily showed connective tissue decomposition and enhanced inflammatory cell infiltration. The TB segment displayed a regular yet loose network of blood clots and fibrous tissue parallel to the bone interface with inflammatory cell infiltration. (Fig. 3D).

2.3.2. 7 Days post-implantation

By day seven, the epithelial tissue, previously descending, began to retract, accompanied by an observable thickening. Connective tissue continued to undergo intense remodeling. A dense osseous interface layer at the bone was a key observation. The RTA's layered remodeling shifted to a structure primarily characterized by immune cells and collagen fibers. In the TE area, a looser inflammatory fibrous structure adhered closely to the epithelium, which showed incomplete basal membrane development and proliferation. The TC area displayed a loose inflammatory fibrous complex closely adhering to the neighboring unremodeled connective tissue. The TB area evolved from a loose coagulation network to a denser collagen matrix with various cells and developing fibers interacting with the bone tissue, which had fewer osteocytes among the groups. (Fig. 3E).

2.3.3. 28 Days post-implantation

By day 28, a pronounced imbalance at the soft-hard tissue interface was evident, marked by connective tissue protrusion and notable bone resorption. Despite the mature structure of the epithelial tissue, it migrated downwards along with the connective tissue. The RTA

persisted, extending its lower edge into the bone tissue. The TE Segment showed increased collagen density and substantial fibroblast presence, with loose connective fibers closely adhering to the mature yet basal membrane-adjacent epithelium, indicating minimal exogenous infection or stimulation. The TC Segment, compared to the PDA group, presented a looser fibrous network with substantial fibroblast infiltration, becoming increasingly lax towards the interface. The TB Segment experienced a disruption in the previous balance, leading to uneven interlocking between connective and bone tissues, extensive infiltration by immune cells and fibroblasts, and a loss of dense bone structure. This interface bone resorption and loss were corroborated by three-dimensional micro-CT results (Fig. S2A). Notably, a significant formation of osteoclasts at the soft-hard tissue interface suggested a trend towards further degradation and downward movement (Fig. 3F, Fig. S3).

2.4. The soft-hard tissue dynamics alterations of PDA/IL4 group

Following the PDA group, we continued to examine the changes in the soft-hard tissue interface balance around metal implants with anti-inflammatory coating modifications at 3-, 7-, and 28 days post-implantation (Fig. 3G–I).

2.4.1. 3 Days post-implantation

In the PDA/IL4 group, a noticeable descent of the epithelial tissue towards the bone interface was observed, paralleled by the formation of a thin dense bone layer at the implant-bone junction. The peri-implant connective tissue revealed a remodeling triangle area (RTA), bounded by neo-epithelium, unremodeled connective tissue, and intact bone, distinct from other groups. The TE Segment exhibited less inflammation, with a dense, mature collagen fiber structure and a well-integrated epithelial basal membrane. The TC Segment primarily showed edematous connective tissue remodeling with increased immune cell recruitment. The TB Segment revealed a dense network of blood clots and fibrous tissue, with intermediate bone affinity, characterized by a thin layer of densification at the bone interface (Fig. 3G).

2.4.2. 7 Days post-implantation

By the seventh day, epithelial retraction was evident, with tissues moving upwards and redefining their positions. The connective tissue around the implant exhibited intense immune cell-rich remodeling, and due to the presence of osteoclasts, the thin dense bone structure at the interface began to diminish. The RTA displayed an inflammatory fibrous complex structure but differed significantly from the other groups in terms of collagen density. The TE Segment showed a denser inflammatory infiltration with continuous epithelial structure. In the TC Segment, a mature, dense collagen fiber network with extensive inflammatory cell infiltration was observed, alongside increased fibroblast and immune cell recruitment in the adjacent unremodeled connective tissue. The TB Segment evolved from a dense blood clot network to a periosteum-like dense collagen matrix structure at the interface (Fig. 3H).

2.4.3. 28 Days post-implantation

By day 28, the PDA/IL4 group achieved the optimal balanced soft-hard tissue interface. This was characterized by non-descending epithelial adhesion, mature and dense connective tissue, and an intact bone surface. Three-dimensional micro-CT data corroborated optimal marginal bone stability (Fig. S2A). Though still visible, the RTA resembled a highly mature and structured normal connective tissue. Specifically, the TE Segment presented the most mature and dense collagen matrix structure of the three groups, supporting the epithelial attachment. The TC Segment also showed a highly mature and dense collagen matrix, with minimal cell recruitment in the adjacent unremodeled connective tissue. Notably, both the TE and TC Segments exhibited abundant fibroblast content, indicative of a healthy biologically active regenerative tissue rather than scarring. In the TB Segment, soft-hard tissue interface balance was observed. The proximal dense connective tissue effectively shielded from exogenous stimuli, and a dense periosteum-like structure near the interface served as a robust soft-hard tissue boundary, mediating a balanced soft-hard tissue interface (Fig. 3I).

2.5. The RTA and transformative effect of immunomodulation

In summary, the formation of the Remodeling Triangle Area (RTA) is intrinsically linked to the surgical procedure of implant placement. The incision and detachment of gingival soft tissue and periosteum create a sharp trauma, leading to edema, inflammation, and remodeling in the surrounding tissues near the incision. Additionally, a space close to the bone surface is occupied by a blood clot, initiating immune cell infiltration and subsequent bone remodeling. The interaction between these remodeling zones forms the RTA, which is crucial for maintaining the soft-hard tissue interface equilibrium. The application of interface immune-coating serves as a crucial tool, not only shedding light on the existence of the remodeling triangle area (RTA) and its boundary behaviors from two different perspectives but also proving instrumental in modulating key factors that govern the equilibrium of the surrounding soft and hard tissues around metal implants. These factors include the strength of epithelial binding, the density of connective tissue, and the intervention in the balance between hard tissue interface rupture and bone formation [31].

Unlike the stable biological width (BW) and Supracrestal Tissue Attachment (STA), which are well-established structure that essential for periodontal and peri-implant health, The Remodeling Triangle Area (RTA) is a dynamic zone at the implant-tissue interface, changing significantly during healing process. BW and STA provide consistent protective structures, while RTA's dynamic and regulatory nature offers a unique opportunity to manage soft-hard tissue equilibrium around implants. Within this zone, the orientation and arrangement of collagen fibers, cellular composition, and the density of inflammatory cells serve as indicators of tissue resilience or susceptibility to ongoing remodeling activities. Notably, the distinct boundary formations and their temporal changes underscore the significance of understanding spatial and molecular interactions within the realm of implantology. While the qualitative insights gained from observing the soft-hard tissue interface dynamics offer foundational knowledge, the absence of quantitative analysis in this study limits our ability to precisely measure the extent of tissue alterations, highlighting an important avenue for future research. It is noteworthy that the separation observed in the Triangle-Bone (TB) region between soft and hard tissues at 3 and 7 days post-implantation in the PDA/IL4 and PDA/LPS/IFNγ groups (Fig. 3D, E, G, H) indicates a lack of robust integration with the bone tissue interface. Our observation at the gingival epithelium-implant interface on the 28-day reveals a robust epithelial attachment and minimal infiltration of inflammatory cells behind the epithelial attachment (Fig. S4). Consequently, this experiment does not encompass the impact of exogenous inflammation around the implant site.

2.6. Distinguished immune characteristics of the RTA under immunomodulation

Subsequent investigations involved collecting soft tissue samples near the implant three days post-implantation for transcriptome sequencing. This analysis highlighted a significant bias in the induction of both innate and adaptive immune responses in the PDA/IL4 group compared to the control group, as evidenced by the enrichment in 80 related Gene Ontology (GO) terms. In contrast, the LPS-treated group primarily exhibited activation of innate immune responses, with only 18 related GO terms identified (Fig. 4A). A closer examination of the PDA/IL4 group revealed that the most enriched immune terms were related to the regulation of T cells (Fig. 4B). A comparative analysis of the top immune term, 'Positive regulation of T cell proliferation,' showed

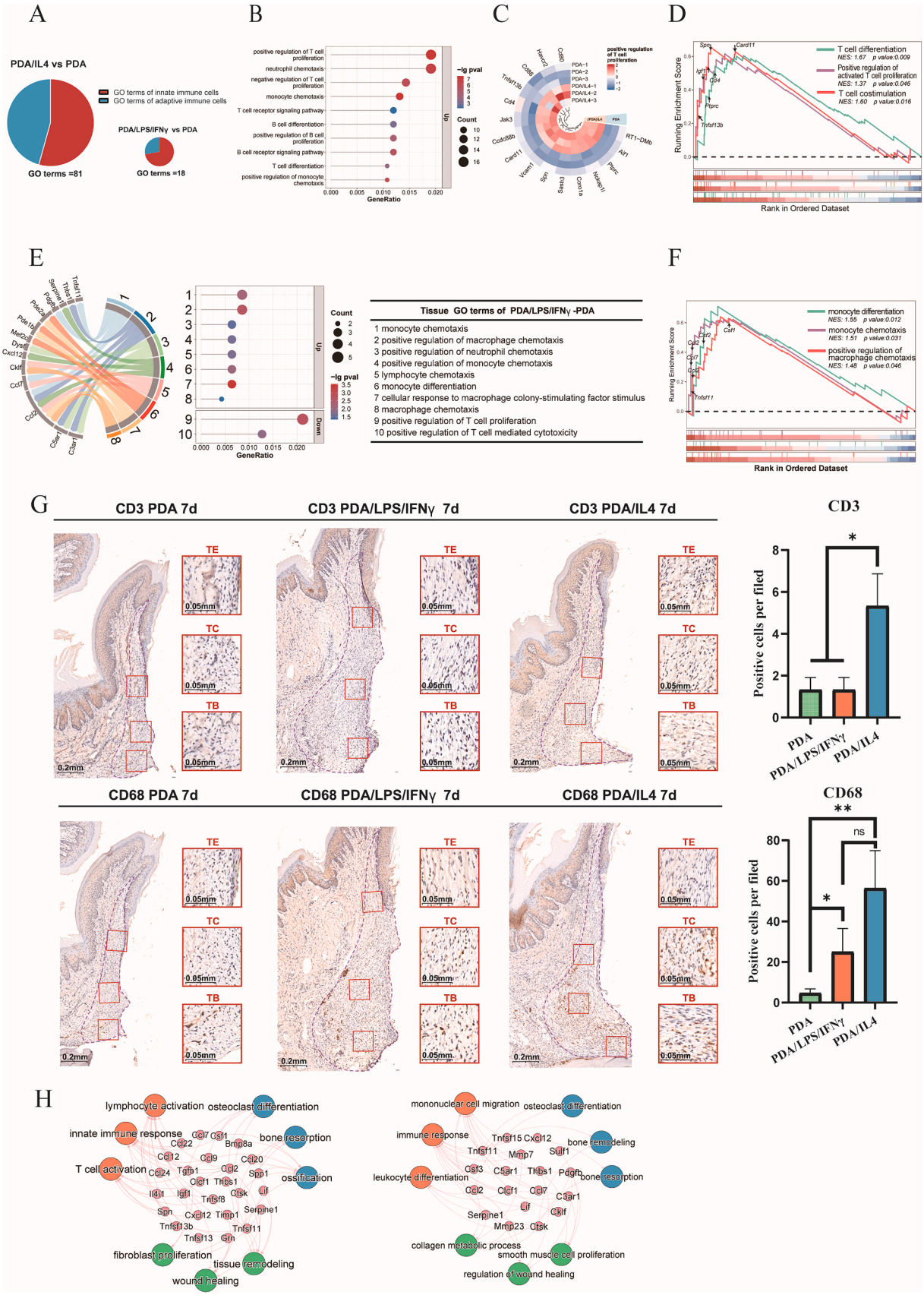

(caption on next page)

Fig. 4. Distinguished immune characteristics of the RTA under immunomodulation. A) A significant bias in the induction of innate and adaptive immune responses in PDA/IL4 group and control group, indicated by GO terms enrichment. B) GO analysis of the PDA/IL4 group revealed the top terms were enriched in the regulation of T and B cells. C) The expression of differential genes of the top functional category 'positive regulation of T cell proliferation' in the PDA/IL4 group. D) GSEA showed the significant upregulation of T cell differentiation, proliferation, and costimulation in the PDA/IL4 group. E) GO analysis of the PDA/LPS/IFNγ group revealed the significant enrichment in chemotaxis and activation of innate immune cells. F) GSEA showed the significant upregulation in monocyte differentiation, chemotaxis, and macrophage chemotaxis in the PDA/IL4 group. G) IHC analysis of the immune environment of RTA at day 7. The semi-quantitative analysis of TC indicated a significant increase in CD3-positive and CD68-positive cells in the PDA/IL4 group. The distribution tendency of these cells were further presented in magnification. H) Enrichment analysis by differential expressed extracellular factors of the PDA/LPS/IFNγ and PDA/IL4 groups compared to the PDA group, respectively. TE, triangle-epithelium; TC, triangle-connective tissue; TB, triangle-bone. $*p < 0.05$, $**p < 0.01$. Red: immune-related terms, green: hard tissue-related terms, blue: soft tissue -related terms. (For interpretation of the references to color in this figure legend, the reader is referred to the Web version of this article.)

significant upregulation in the PDA/IL4 group compared to the control with a considerable increase in the expression of relevant genes (Fig. 4C). Gene Set Enrichment Analysis (GSEA) (Fig. 4D, Fig. S6A) indicated notable upregulation in the PDA/IL4 group in terms of T cell survival and activation functions, including 'Positive regulation of activated T cell proliferation,' 'T cell differentiation,' and 'T cell costimulation' ($p < 0.05$). Essential adaptive immune-related genes such as *Tnfsf13b*, *Spn*, *Crad11*, *Ptprc* and *Igf1*, *etc.* were also upregulated. For the PDA/LPS/IFNγ group, the most enriched immune terms were related to chemotaxis and activation of innate immune cells such as monocytes, macrophages, and neutrophils, with core term genes identified by the chord diagram; it is evident that *Ccl2* has the most extensive influence. (Fig. 4E). GSEA (Fig. 4F, Fig. S6B) showed significant upregulation in 'positive regulation of macrophage chemotaxis,' 'monocyte differentiation,' and 'monocyte chemotaxis,' with upregulation of classic innate immune-regulatory genes like *Ccl2*, *Ccl7*, *Csf2*, and *Tnfsf11*.

Seven days post-implantation, immunohistochemistry elucidated the immune cell topography within the 'remodeling triangle area' (Fig. 4G). The PDA/IL4 group exhibited the highest prevalence of CD3-positive T cells, predominantly distributed at the core of the remodeling zone, exceeding the numbers found in the PDA/LPS/IFNγ and PDA groups. The most substantial accumulation of CD68-positive macrophages was observed in the PDA/IL4 group. The PDA/LPS/IFNγ group showed an increase in CD68-positive cells compared to controls but fewer than in the IL4 scenario. Spatial analysis indicated a distribution of these cells across the RTA, with a tendency to cluster closer to the body and bone interface than the epithelial boundary. We performed enrichment analysis by the differential expressed extracellular factors in the immune microenvironment of the PDA/LPS/IFNγ and PDA/IL4 groups compared to the PDA group, respectively (Fig. 4H). Terms related to immune, hard tissue, and soft tissue were closely intersected through shared key factors. Quantitative comparisons of related factors were further illustrated in Figs. S5A–B.

We have employed histological and genomic approaches to describe the pronounced fluctuation in the immune environment around metal implants from various perspectives. The 3-day time point was chosen for transcriptome analysis to capture early gene expression changes during the acute inflammatory phase, while the 7-day time point for IHC analysis was selected to evaluate tissue remodeling and immune cell infiltration during the intermediate healing phase. These timings provide comprehensive insights into the dynamic processes within the RTA, ensuring robust and relevant findings for both molecular and histological evaluations. The immune engagement in the PDA/LPS/IFNγ group is predominantly driven by innate mechanisms. In contrast, at seven days, the PDA/IL4 group demonstrates a synergistic enhancement of both adaptive and innate immune responses. The further immunohistochemical analysis contributes to our spatial understanding of these dynamics, revealing an overwhelming distribution of immune cells within the RTA of connective tissue, especially at the core of the remodeling zone and bone tissue juncture.

Notably, in this study, the PDA/IL4 group exhibits a relatively more robust adaptive immune process compared to the PDA/LPS/IFNγ group, with T cell activation being a primary characteristic. Research also suggests that, in comparison to periodontitis, T lymphocytes play a dominant role in healthy oral mucosa [32], while innate immune cells, such as macrophages, play a crucial role in inflammatory responses around implants [33]. This comprehensive evidence emphasizes the essential role of balanced and coordinated adaptive and innate immune responses in the healthy equilibrium of the soft-hard tissue interface [34]. The regulation of the delicate balance between destructive and protective immune responses by adaptive and innate immunity is complex, necessitating further detailed research for elucidation [35].

2.7. RTA governs peri-hard tissue via distinguished immune microenvironments

To further elucidate the regulatory effects of the immune microenvironment changes in the PDA/IL4 and PDA/LPS/IFNγ groups on hard tissue, we conducted an analysis of osteo-immune regulatory function annotation heatmaps for both groups (Fig. 5A). In the PDA/IL4 group, relative to the control group, 21 upregulated exocrine differential factors were identified. These factors not only possessed monocyte chemotaxis, T cell activation, and neutrophil chemotaxis functions related to innate/adaptive immune regulation but also played roles in osteoclast/osteoblast differentiation, bone resorption regulation, and bone mineralization, contributing to osteo-regulatory functions. In contrast, the PDA/LPS/IFNγ group showed upregulation of 13 exocrine differential factors, primarily involved in macrophage chemotaxis, monocyte chemotaxis, and innate immune regulation, as well as osteoclast/osteoblast differentiation and bone resorption control. Notably, RANKL (namely TNFSF11), a classic factor antagonizing OPG in regulating osteoclast-osteoblast balance, was significantly upregulated in expression in both groups.

To delve deeper into the expression and spatial distribution of RANKL and its antagonist OPG at the protein level across three groups, we conducted immunohistochemical analyses in the remodeling triangle area of the metal implant seven days post-implantation. In the control group, RANKL-positive cells were sparsely distributed in the body of the remodeling area (TC), the bone interface (TB), and the epithelial junction (TE). In the PDA/LPS/IFNγ group, a more pronounced distribution of RANKL was observed in all three areas compared to the control group, with substantial RANKL presence noted not only in TC but also at the TB interface. Conversely, the PDA/IL4 group exhibited similar levels of RANKL expression at the TC, but notably less in the TB region compared to the PDA/LPS/IFNγ group (Fig. 5B). Consistent results were presented by the RT-qPCR analysis, which showed a significant increase in RANKL relative expression in the PDA/LPS/IFNγ group compared to the PDA group ($p < 0.05$), while the difference between the PDA/IL4 and PDA groups was not significant (Fig. S5C). Regarding OPG expression, minimal levels were observed in the control and PDA/LPS/IFNγ groups across all three areas. However, the PDA/IL4 group showed a significant increase in OPG expression at both the TB and TC of the remodeling area (Fig. 5C). Correspondingly, the RT-qPCR analysis demonstrated a significant increase in OPG relative expression in the PDA/IL4 group compared to the PDA and PDA/LPS/IFNγ groups ($p < 0.05$), while the difference between PDA and PDA/LPS/IFNγ groups was not significant (Fig. S5D).

RANKL and OPG are crucial regulators in osteoclast development and function, significantly influencing alveolar bone resorption [36,37]. Our findings indicate that the PDA/LPS/IFNγ group demonstrates a

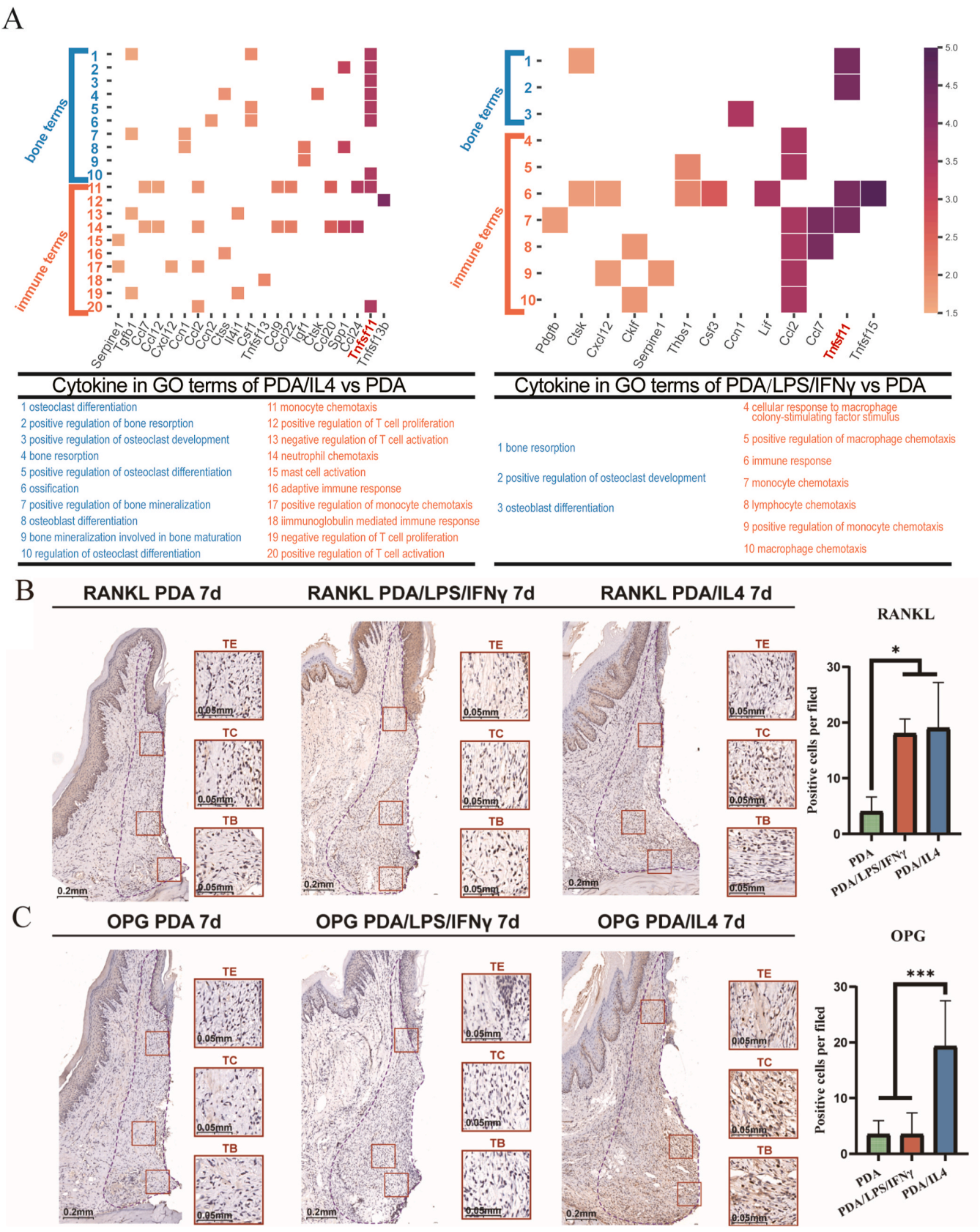

Fig. 5. RTA governs peri-hard tissue via distinguished immune microenvironments A) GO analysis concerning the osteo-immune regulatory effect of cytokines in PDA/IL4 and PDA/LPS/IFNγ groups. B–C) IHC analysis conducted at day 7 post-implantation, illustrating the differential expression and spatial distribution of RANKL and OPG in the internal structure of RTA: TE (triangle-epithelium), TB (triangle-bone), and TC (triangle-connective tissue) across three groups. The semi-quantitative analyses of RANKL and OPG were conducted in TB zone. $*p < 0.05$, $***p < 0.001$.

pronounced expression of RANKL with comparatively low OPG levels at the bone interface within the remodeling zone, leading to a skewed OPG/RANKL ratio that promotes bone resorption. This skewed balance is a critical contributor to the active bone resorption and notable bone tissue loss observed at the soft-hard tissue interface 28 days post-implantation, as shown in Fig. S3. Conversely, in the PDA/IL4 group, despite the high levels of RANKL, the substantial concurrent presence of OPG achieves a more balanced osteoclastic and osteoblastic activity. This balance is likely fundamental to the group's balanced soft-hard tissue interface, highlighting a reduced focus on bone resorption processes. (Fig. 5C).

An optimal microenvironment is crucial in the processes of bone regeneration and bone healing [38,39]. Existing studies indicate that various immune cells, including T cells, B cells, macrophages, osteoblasts, and gingival fibroblasts, can produce RANKL. *In vitro* experiments have reported diverse results; for instance, Wada et al. found that LPS stimulates fibroblasts to secrete more OPG than RANKL, inhibiting osteoclast differentiation and activity [40]. Koehler et al. observed that fibroblasts cultured alone show high OPG and low RANKL levels, promoting a bone-protective state [41]. *In vivo* studies have shown increased RANKL concentrations in the peri-implant mucositis group compared to the peri-implant health group, with the lowest median concentration of OPG in the peri-implantitis group [42]. This aligns with our experiment's observation of elevated RANKL and minimal OPG production in the PDA/LPS/IFNγ group. The PDA/LPS/IFNγ group seems to mimic, through clever immune modulation, aspects of the peri-implantitis immune microenvironment during the early stages of implantation. This aligns with Albrektsson et al.'s observations that immune imbalance, even without bacterial presence, can lead to marginal bone resorption [43]. Based on our study's continuous pathophysiological observations, we hypothesize that changes in the immune architecture of the 'Remodeling Triangle Area' might be the fundamental etiology of 'peri-implantitis due to soft tissue immune imbalance'. Our findings that an adaptive immune-dominated microenvironment (PDA/IL4 group) favors soft-hard tissue interface equilibrium compared to an innate immune-dominated microenvironment (PDA/LPS/IFNγ group) align with existing studies. These studies have shown that excessive innate immune responses can lead to chronic inflammation and tissue degradation, making it more difficult to transition to an adaptive immune-dominated phase. In contrast, adaptive immune responses, particularly those involving regulatory T cells (Tregs), support tissue regeneration and stability. These studies suggest that enhancing adaptive immunity may be a crucial strategy for achieving long-term tissue integration around implants.

2.8. Regulatory mechanism of immune changes in RTA on peri-metal implant soft tissues

To further uncover the regulatory mechanism of the immune microenvironment alterations in the PDA/IL4 and PDA/LPS/IFNγ groups on soft tissue, we analyzed the soft tissue regulation-immune regulation functional annotation heatmaps for both groups (Fig. 6A). The PDA/IL4 group, relative to the control, upregulated 29 exocrine differential factors, which not only encompass monocyte chemotaxis, T cell proliferation and activation, and neutrophil chemotaxis—functions related to innate/adaptive immune regulation—but also facilitate fibroblast migration, collagen biosynthesis, and wound healing, contributing to soft tissue regulation. The PDA/LPS/IFNγ group upregulated 15 exocrine differential factors, mainly involved in macrophage chemotaxis, monocyte chemotaxis, cell adhesion, collagen biosynthetic process, and actin filament polymerization.

Given the complexity of soft tissue behavior, we paid particular attention to factors with multifaceted roles in soft tissue regulation. Importantly, IGF1, a key regulator of soft tissue healing, showed significant regulatory effects on fibroblast proliferation, collagen synthesis, and myofibroblast differentiation, essential for connective tissue-implant quality (Fig. 6C). Our team has also previously identified its role in activating the PI3K-AKT pathway, promoting semi-desmosome adhesion between epithelium and implant [19]. Wang et al. enhanced epithelial cell proliferation and adhesion by using a Lactoferrin-Derived Amyloid Coating, which activated the PI3K-AKT pathway [44]. Similarly, in this study, PI3K-AKT pathway activation was observed, and its contributing genes are illustrated in Fig. 6D, all of which are associated with the aforementioned regulation of soft tissue functions. To explore the expression and spatial distribution of IGF1 at the protein level, we conducted immunohistochemical analysis in the remodeling triangle area of the metal implant seven days post-implantation. The control group showed widespread IGF1 distribution at the epithelial junction, body, and bone interface of the remodeling area (Fig. 6B). The semi-quantitative analysis of TC, a critical region for subsequent connective tissue integration, showed a significant increase in IGF1-positive cells in the PDA/IL4 group compared to the PDA and PDA/LPS/IFNγ groups, with PDA also showing a significant increase compared to PDA/LPS/IFNγ. We also conducted RT-qPCR analysis to explore the expression difference of IGF1 at mRNA level. Results demonstrated a significant increase in IGF1 relative expression in the PDA/IL4 group compared to the PDA and PDA/LPS/IFNγ groups ($p < 0.05$), while the difference between PDA and PDA/LPS/IFNγ groups was not significant (Fig. S5E).

2.9. Regulatory effect of immune changes in RTA on peri-metal implant soft tissues

We further evaluated the functional changes of peri-metal implant soft tissues. A closer examination of the PDA/IL4 group in relation to the control revealed the highest enrichment in soft tissue healing-related terms, with extracellular matrix organization being the most significantly enriched (Fig. 7A). Further analysis of the expression patterns of the genes comprising this term clearly demonstrates enhanced expression of soft tissue healing-related genes (Fig. 7B). GSEA analysis (Fig. 7C, Fig. S7A) showed notable upregulation in the PDA/IL4 group in 'Crosslinking of Collagen Fibrils,' 'Collagen Formation,' and 'Extracellular Matrix Organization,' with crucial collagen remodeling genes such as *Col1a1*, *Col3a1*, *Tgfb1*, *Serpinh1* and *Timp1* also upregulated. In an alternative enrichment analysis, we found that the wound healing term and cell adhesion were activated, while the keratinocyte differentiation term was suppressed. The Laminin5 is the main component of hemidesmosomes in the junctional epithelium Then, the HE-stained immunofluorescence localization revealed that the PDA/IL4 group had significantly stronger expression of Laminin5, a critical protein for hemidesmosome-related epithelial adhesion [45], than the other groups, indicating the strongest epithelial binding capacity in the PDA/IL4 group (Fig. 7D). FN, an essential fibroblast-related adhesion molecule and a main component of ECM, was most abundantly expressed in the PDA/IL4 group, particularly concentrated in the connective tissue integration area (Fig. 7E). After 28 days, the PDA/IL4 group also facilitated the formation of the densest and most mature collagen network.

Fig. 7F demonstrates that the highest enrichment of soft tissue healing-related terms in the PDA/LPS/IFNγ group was associated with processes such as smooth muscle contraction (as depicted in the gene heat map inFig. S7C), extracellular matrix degradation, and activation of matrix metalloproteinases, among others. GSEA further revealed significant upregulation in the PDA/LPS/IFNγ group in the 'smooth muscle contraction' term, with key contraction-related genes such as *Acta2, Mylk, Tpm1*, and Actg2 also exhibiting upregulation (Fig. 7G, Fig. S7B). The inhibition of keratinocyte differentiation observed at 3 days post-implantation in PDA/IL4 group (Fig. S8A) reflects a critical phase of rapid epithelial proliferation and migration necessary for initial wound healing. This temporary suppression supports early protective layer formation. Moreover, subsequent observations at 28 days post-implantation show the epithelial tissue in PDA/IL4 group exhibits best

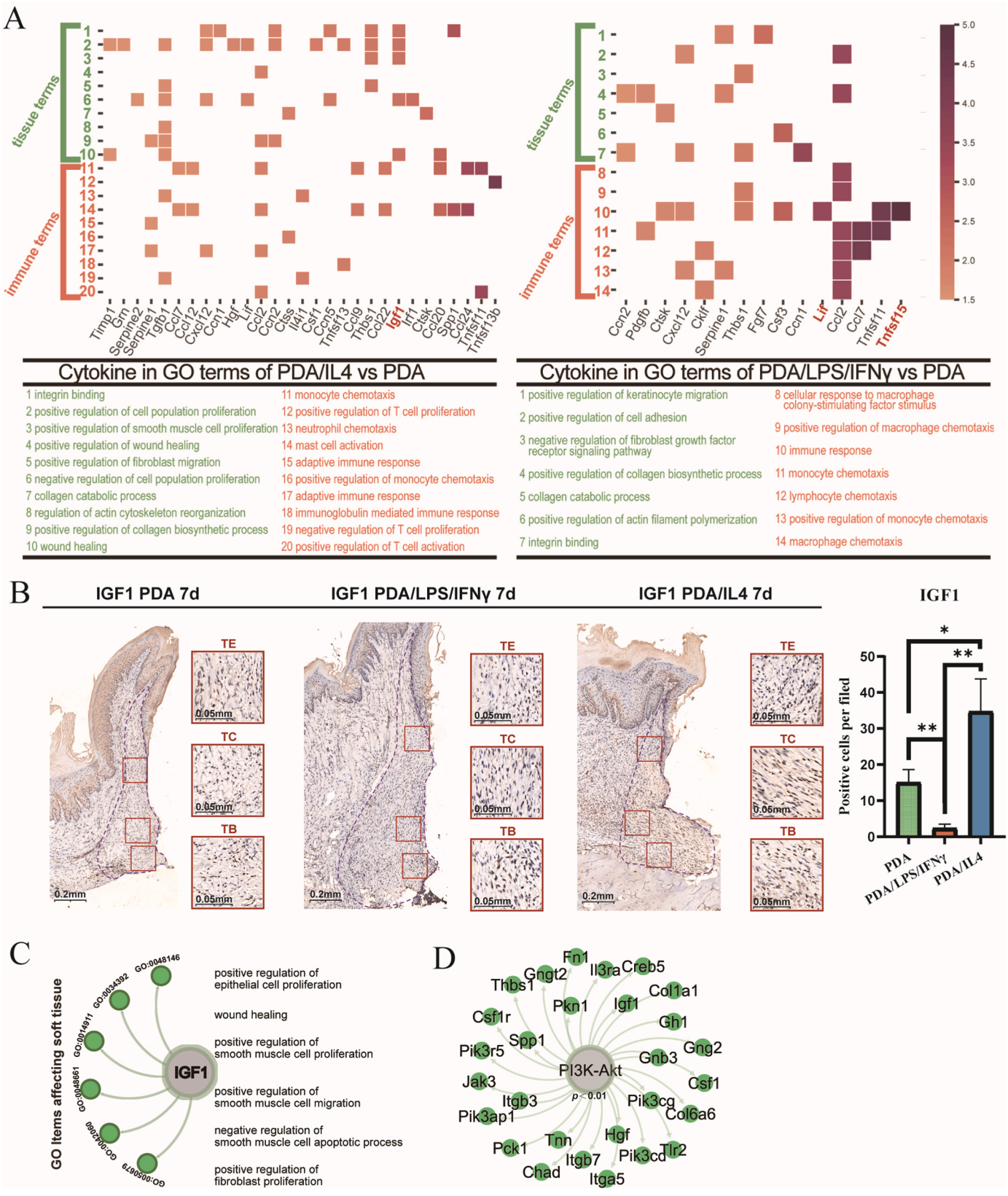

Fig. 6. Regulatory mechanism of immune changes in RTA on peri-metal implant soft tissues. A) GO analysis concerning the soft tissue-immune regulatory effect of cytokines in PDA/IL4 and PDA/LPS/IFNγ groups. B) IHC analysis of the soft tissue healing environment of the RTA at day 7. The IHC semi-quantitative analysis of TC showed a significant increase in IGF1-positive cells in the PDA/IL4 group compared to the PDA and PDA/LPS/IFNγ groups, with PDA also showing a significant increase compared to PDA/LPS/IFNγ. C) IGF1 related GO terms affecting soft tissue. D) Differential genes involved in PI3K-Akt pathway. TE, triangle-epithelium; TC, triangle-connective tissue; TB, triangle-bone. $*p < 0.05$, $**p < 0.01$.

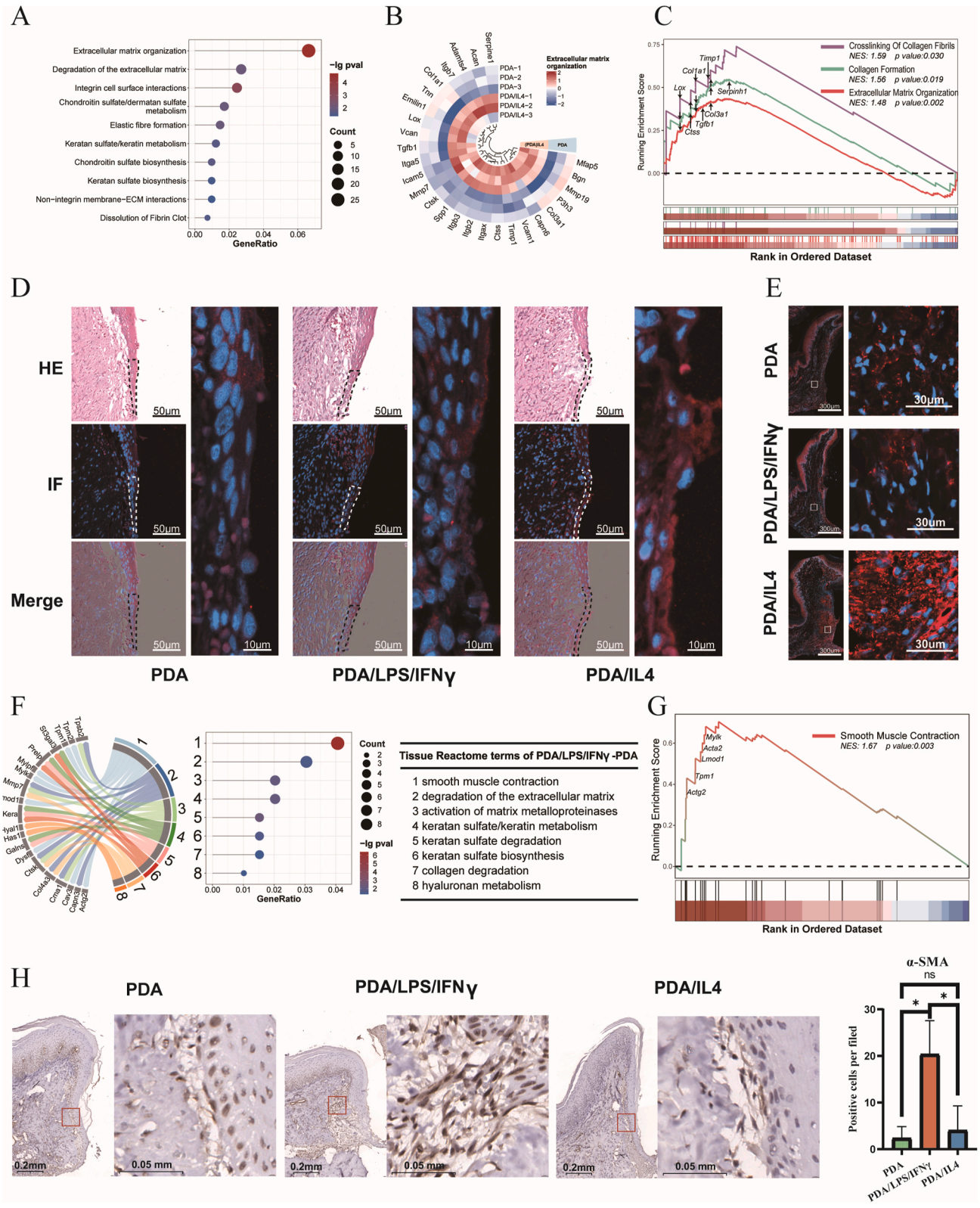

Fig. 7. Regulatory effect of immune changes in RTA on peri-metal implant soft tissues. A) GO analysis showed the highest enrichment in soft tissue-related terms in the PDA/IL4 group. B) The expression of differential genes of the top functional term 'extracellular matrix organization' in the PDA/IL4 group. C) GSEA showed the significant upregulation of collagen fibrils crosslinking, collagen formation, and extracellular matrix organization in the PDA/IL4 group. D) Typical images of H&E and laminin5 immunofluorescence staining of the three studied groups at 28-day post-implantation. The PDA/IL4 group exhibited stronger expression of laminin5. E) Immunofluorescence staining showed the highest expression of FN1 in the PDA/IL4 group at 7-day post-implantation. F) Reactome analysis revealed the highest enrichment of soft tissue-related terms in the PDA/LPS/IFNγ group. G) GSEA showed the significant upregulation of smooth muscle contraction in the PDA/LPS/IFNγ group. H) IHC analysis of soft tissue contraction of the RTA at 3-day post-implantation. The semi-quantitative analysis revealed the highest level of α-SMA expression in the PDA/LPS/IFNγ group. $^{*}p < 0.05$.

integration property (Fig. 7D), indicating that initial differentiation inhibition benefits early healing and does not compromise long-term soft tissue quality. Additional α-SMA immunohistochemical staining provided further confirmation of a higher number of α-SMA positive cells in the body of the remodeling area in the PDA/LPS/IFNγ group compared to the other groups (Fig. 7H). In the immune-related microenvironment influenced by the PDA/LPS/IFNγ group, there was an upregulation of factors such as *Tnfsf15* and *Lif*, coupled with the lowest secretion of IGF1 among all groups studied (Fig. 6A and B). Previous studies have revealed that IGF1 inhibits the differentiation of fibroblasts into α-SMA positive cells. Conversely, factors like *Tnfsf15* and *Lif* are known to promote this differentiation [46,47]. This observation suggests the group's superior soft tissue contraction capability, setting it apart from the enhanced adhesion and healing properties observed in the PDA/IL4 group (Fig. S8B). In addition, we further observed the association between the expression of factors within the immune microenvironment and the expression of functional proteins. Correlation analysis showed that the difference between the two groups was highly related to the differences in factors within the immune microenvironment (Fig. S9). It is noteworthy that this finding contradicts our earlier *in vitro* experiments, where the PDA/IL4 group was reported to promote fibroblast differentiation and cell contraction behavior [31]. This inconsistency may arise from the simplified culture conditions, lacking the temporal and spatial complexity of cellular interactions. Furthermore, tissue-specific differences and the timing of IGF-1 expression can result in varying outcomes. It underscores the importance of delineating the precise pathways and interactions that govern IGF-1 signaling and its effects on myofibroblast differentiation in various tissues.

2.10. RTA-focused immunomodulation strategy for advanced metal implants with soft-hard management property

Metal implants represent a groundbreaking collaborative material for soft and hard tissues, holding significant promise in various fixed prostheses. However, imbalances at the soft-hard tissue interface currently limit their extended reliability and broader application. Utilizing immune-modulatory coatings, our study highlights the formation and function of the 'Remodeling Triangle Area' (RTA), which is crucial for maintaining equilibrium between soft and hard tissues. We demonstrate the contrasting regulatory effects of PDA/IL4 and PDA/LPS/IFNγ coatings on the RTA and consequently the soft-hard tissue interface equilibrium (Fig. 8). Our results are applicable to a wide range of implants, including dental implants, orthopedic fixation devices, and other perforating biomedical implants. By leveraging the RTA-focused immunomodulatory approach, we can design novel implants with better soft-hard tissue interface equilibrium property, thereby enhancing their performance and longevity.

Building on these findings, future work should focus on deepening the understanding of the RTA and its interactions with biomaterials. This should begin by exploring the relationship between different biomaterial properties and the RTA, such as investigating various interface modifications (*e.g.*, roughness, hydrophilicity, surface morphology,

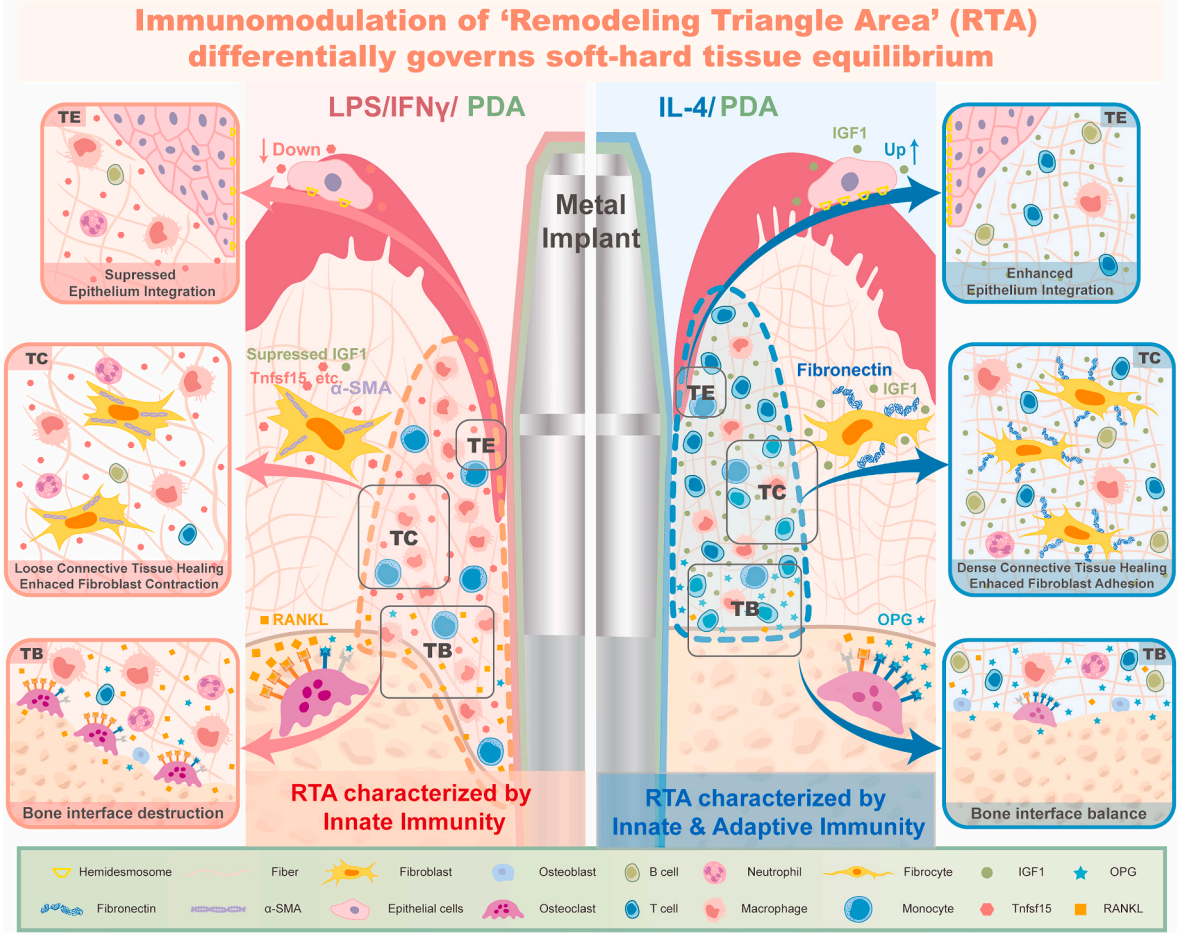

Fig. 8. Schematic diagram shows the governing role of 'remodeling triangle area' in soft and hard tissue equilibrium for metal implants advancement. The different coatings of the implants generate different remodeling triangle areas (RTAs), which further govern the soft and hard tissue equilibrium. The PDA/IL4 coating activates innate and adaptive immune responses with increased IGF1 secretion, and generates a balanced soft-hard tissue interface. The PDA/LPS/IFNγ coating activates innate immunity with reduced IGF1 secretion, and generates a lower-quality soft-hard tissue interface.

surface charge, and chemical coatings) to elucidate their impact on immune cell behavior within the RTA. More importantly, comprehensive, high-throughput molecular biology techniques should be employed to reveal the molecular mechanisms by which the RTA's internal immune structure regulates critical functions such as epithelial adhesion, fibroblast proliferation, collagen synthesis, and bone remodeling. Meanwhile, it's noteworthy that the tendon interface, another nature soft-hard tissue interface, also faces challenges related to equilibrium of soft and hard tissues during injury repair. However, tendon interfaces involve unique mechanisms such as gradient transitions and fiber insertions that require further study.

Based on an in-depth understanding of the molecular biological mechanisms by which the RTA regulates surrounding tissues, it is important to consider that direct implant coatings might have direct effects on tissue cells, potentially introducing confounding influences. Therefore, future strategies could involve more direct biological interventions, such as the injection of bioactive agents directly into the RTA region. Developing precise regulatory strategies for the RTA, and creating and testing materials that can specifically modulate the RTA to achieve a balanced soft-hard tissue interface, will ultimately enhance the long-term reliability and functionality of metal implants.

3. Conclusions

Our study establishes the 'Remodeling Triangle Area' (RTA) as a pivotal factor in governing soft-hard tissue interface equilibrium around metal implants, especially highlighting the transformative effect of immunomodulation. We demonstrate that the RTA can be influenced by PDA/IL4 coating to favor a phenotype that enhances both innate and adaptive immune responses, leading to improved soft tissue seal and bone stability, mediated by mechanisms such as IGF1 secretion and the OPG/RANKL system. In contrast, the PDA/LPS/IFNγ coating, while stimulating innate immunity of RTA, adversely affects the balance. The RTA-centered immunomodulation approach demonstrated may not only reshape the paradigm for soft-hard tissue interface equilibrium challenges but also significantly accelerate the advancement of next-generation metal implants with unparalleled soft-hard tissue interface equilibrium property.

4. Materials and methods

4.1. Materials preparation and characterization

The mini-implants were first immersed in EP tubes containing 48 mL of PDA (2 mg mL^{-1}) solution at 37 °C for 24 h. The PDA-coated micro-implants were then transferred to EP tubes containing 16 mL of IL4 (500 ng mL^{-1}) solution or 16 mL of LPS (10 μg mL^{-1}) + IFNγ (200 ng mL^{-1}) solution at 4 °C for 24 h. The micro-implants were then removed and placed in moist EP tubes at 4 °C for implantation surgery. The concentration of LPS, IFNγ and IL4 in the remaining solution was measured by ELISA kit according to the manufacturer's instruction. SEM and XPS were used to verify the coatings. The coated implants were used for *in vivo* study.

4.2. Surgical procedures

Animal procedures were approved by the Institutional Animal Care and Use Committee (IACUC), Sun Yat-sen University (approval no. SYSU-IACUC-2022-000437) and were performed in accordance with the guidelines approved by the Animal Ethical and Welfare Committee of Sun Yat-sen University. 8 weeks-old male Sprague Dawley rats (SD rats) weighing 250–300 g were used. 24 rats (with a total of 48 implants) were randomly divided into four groups. Group 1 (n = 6 rats, 12 implants) was used for 3-day transcriptomic sequencing analysis, and randomly divided into PDA, PDA/IL4, and PDA/LPS/IFNγ subgroups (2 rats per subgroup, 4 implants per subgroup). Groups 2, 3, and 4 (n = 6 rats each, 12 implants each) were used for histopathological studies at 3 days, 7 days, and 28 days, respectively. Each group further divided into PDA, PDA/IL4, and PDA/LPS/IFNγ subgroups (2 rats per subgroup, 4 implants per subgroup). Excluded any implants showing signs of loosening or detachment. The animals were anesthetized using zoletil50 (0.1 mL per 100 g) and the bilateral maxillary first molars were removed. 4 weeks later, the soft and hard tissues of the tooth extraction socket were healed. The animals were anesthetized again, and the implant holes were prepared via twist drill. The mini-implants were implanted in the prepared implant holes with screwdriver and the surrounding soft tissues were sutured. One-half of the animals were allowed to heal for 3 days, and the other quarters of the animals were allowed to heal for 7 days and 4 weeks, respectively. Then they were killed under excessive anesthesia. Half of the rats in the three-day group will be used for gingival resection for mRNA extraction. 1 mm of gingival tissue around the rat implant was cut. These specimens were composed of peri-implant epithelial tissue and connective tissue, and were recovered and stored in RNAlater (ThermoFisher, Rochester, NY). For these remaining groups of rats, the mini-implants and the maxillary bones containing soft and hard tissues were removed at 3 days, 7 days, and 4 weeks, respectively. These samples were then fixed in 4 % PFA.

4.3. Histological analysis

Tissue samples were collected on day 3, 7, and 28 after surgery. Samples were fixed in 4 % paraformaldehyde solution that buffered by 0.1 M phosphate solution for 24 h and then decalcified in 4 % EDTA for 6 weeks. Tissue samples were stained by Mayer's hematoxylin (Servicebio, China) and eosin (Servicebio, China). For IHC staining, the slides were blocked with a 5 % BSA (Macklin, China) solution for 1 h and incubated with CD68 antibody (1:200; ab125212, Abcam), CD3 antibody (1:200; ab16669, Abcam), RANKL (1:300; bs-0747R, Thermo Fisher), OPG (1:300; ab183910, Abcam), α-SMA antibody (1:2000; ab7817, Abcam), IGF1 antibody (1:600; ab9572, Abcam), after antigen retrieval. The sections were then incubated with a secondary antibody (Genetech, China) for 1 h at room temperature. The diaminobenzidine solution (Genetech, China) and Mayer's hematoxylin were used to stain the antigen-antibody complexes and the nuclei. Images were captured using Aperio AT2 system (Leica Aperio AT2, Germany) and Slideviewer software.

4.4. Immunofluorescence staining

Paraffin sections were stained by 4',6-diamidino-2-phenylindole (DAPI) simultaneously with FN1 (1:1000; ab268020, Abcam), L5α3 (1:200; ab217213, Abcam), IGF1 antibody (1:600; ab9572, Abcam) for different purposes. The sections were incubated with Alexa Fluor 647 goat anti-rabbit secondary antibody (Beyotime, China) at room temperature for 1 h. Fluorescent images were observed using the confocal laser scanning microscope (Zeiss LSM 980, Germany).

4.5. mRNA sequencing

Total RNA was extracted using the TRIzol reagent (Invitrogen, CA, USA) according to the manufacturer's protocol. RNA purity and quantification were evaluated using the NanoDrop 2000 spectrophotometer (Thermo Scientific, USA). RNA integrity was assessed using the Agilent 2100 Bioanalyzer (Agilent Technologies, Santa Clara, CA, USA). Then the libraries were constructed using VAHTS Universal V6 RNA-seq Library Prep Kit according to the manufacturer's instructions.

The transcriptome sequencing were conducted by OE Biotech Co., Ltd. (Shanghai, China). The library was sequenced using an Illumina Novaseq 6000 sequencing platform, and 150 bp paired-end reads were generated. Use FASTQ to process the raw reads, remove low-quality reads and obtain clean reads. Each sample obtained approximately 50M raw reads for subsequent data analysis. Use HISAT2 software to

perform reference genome comparison and calculate gene expression (FPKM).

4.6. Differentially expressed genes analysis

Differentially expressed genes were analyzed where genes meeting the thresholds of q value < 0.05 and Foldchange >1.5 or foldchange $<2/3$ were defined as differentially expressed genes (DEGs). Hierarchical clustering analysis of DEGs was performed to demonstrate the expression patterns of genes in different groups and samples. The hypergeometric distribution algorithm based on the R package was used to conduct GO, KEGG, and Reactome enrichment analysis of differentially expressed genes, and was used to screen significant enrichment functional entries. Draw a bar chart, chord chart, term-gene heatmap, or enrichment analysis bubble chart for significant enrichment feature entries. Gene set enrichment analysis was performed. Using a predefined gene set, genes are sorted according to their differential expression levels in two types of samples, and then the enrichment score (ES), significance level of ES and the "gene tags" of the target gene set were observed. For genes of interest, correlation matrix analysis between cytokine expression levels and correlation matrix analysis between cytokine expression levels and functional proteins were performed. R (v 4.3.2) and python (v 3.10.10) were used for downstream analysis and visualization of the differentially expressed gene analysis mentioned above. R packages used: clusterProfiler(4.10.0), ReactomePA(1.46.0), org.Rn.eg.db(3.18.0),circlize (v 0.4.15), enrichplot (v 1.22.0), corrplot (0.92), ggplot2 (v 3.4.4), and RColorBrewer(1.1–3). Python packages used: numpy(1.26.0), pandas(2.1.1), matplotlib(3.8.0) and seaborn (0.12.2).

4.7. CT measurements and analysis

Maxillary bone samples of the 4-week group were scanned using Micro-CT (VENUS, PINGSENG Healthcare Inc.) at 10 μm resolution. First, the rat maxilla was placed in the sample chamber, the scanning tube voltage was set to 60 kV, the tube current was set to 120 μA. The detector and tube then rotated 360° around the central axis of the sample chamber. During the scanning process, each sample scanning area was projected 10,000 times. Images captured by the detector are transferred to a computer and reconstructed using the FDK method in reverse with a voxel of 8 μm × 8 μm × 9 μm in Avatar software (v1.7.6.1, PINGSENG Healthcare Inc.). After reconstruction, the three-dimensional structure of the bone around the maxillary implant was analyzed to evaluate changes in bone quality and bone mass between different groups using NRecon software (v1.7.6.1, PINGSENG Healthcare Inc.). Bone volume fraction (BV/TV,%), bone mineral density (BMD).

4.8. Statistical analysis

The bioinformation analysis statistical results were provided directly by the R or Python packages. The unpaired two-tailed Student's t-test was adopted to assay the difference between groups using the GraphPad Prism (version 9.5.1). Differences were considered significant if $p < 0.05$.

CRediT authorship contribution statement

Shoucheng Chen: Writing – original draft, Visualization, Methodology, Investigation, Funding acquisition, Data curation, Conceptualization. **Guangqi Gao:** Writing – original draft, Visualization, Validation, Methodology, Investigation, Formal analysis, Data curation, Conceptualization. **Jiamin Shi:** Writing – original draft, Validation, Investigation, Data curation. **Na Li:** Writing – original draft, Visualization, Investigation, Data curation. **Lv Xie:** Validation, Methodology, Investigation, Data curation. **Yingye Zhang:** Visualization, Investigation. **Zhengjie Shan:** Methodology, Investigation. **Jiaxin Xie:** Visualization, Investigation. **Yin Xiao:** Writing – review & editing, Supervision, Funding acquisition, Conceptualization. **Zhuofan Chen:** Writing – review & editing, Supervision, Funding acquisition. **Zetao Chen:** Writing – review & editing, Supervision, Project administration, Funding acquisition, Conceptualization.

Declaration of competing interest

The authors declare no conflict of interest.

Data availability

Data will be made available on request.

Acknowledgements

This work was financially supported by National Key R&D Program of China (2022YFA1104400), National Natural Science Foundation of China (82201119, 82071167, 81970975), Guangdong Basic and Applied Basic Research Foundation (2023A0505050138, 2021A1515110380), Guangzhou Basic and Applied Basic Research Scheme (2024A04J6323), Fundamental Research Funds for the Central Universities (22ykqb06), Guangdong Financial Fund for High-Caliber Hospital Construction, AO Research Grant.

Appendix A. Supplementary data

Supplementary data to this article can be found online at https://doi.org/10.1016/j.mtbio.2024.101170.

References

[1] R. Davis, A. Singh, M.J. Jackson, R.T. Coelho, D. Prakash, C.P. Charalambous, W. Ahmed, S.L. Da, A.A. Lawrence, A comprehensive review on metallic implant biomaterials and their subtractive manufacturing, Int. J. Adv. Manuf. Technol. 120 (2022) 1473–1530.
[2] Y. Su, H. Yang, J. Gao, Y.X. Qin, Y. Zheng, D. Zhu, Interfacial zinc phosphate is the key to controlling biocompatibility of metallic zinc implants, Adv. Sci. 6 (2019) 1900112.
[3] M. Ortiz-Catalan, B. Hakansson, R. Branemark, An osseointegrated human-machine gateway for long-term sensory feedback and motor control of artificial limbs, Sci. Transl. Med. 6 (2014) 257re6.
[4] M.N. Abdallah, Z. Badran, O. Ciobanu, N. Hamdan, F. Tamimi, Strategies for optimizing the soft tissue seal around osseointegrated implants, Adv. Healthcare Mater. 6 (2017).
[5] J. Hou, Z. Xiao, Z. Liu, H. Zhao, Y. Zhu, L. Guo, Z. Zhang, R.O. Ritchie, Y. Wei, X. Deng, An amorphous peri-implant ligament with combined osteointegration and energy-dissipation, Adv. Mater. 33 (2021) e2103727.
[6] J. Zhang, Y. Zhuang, R. Sheng, H. Tomas, J. Rodrigues, G. Yuan, X. Wang, K. Lin, Smart stimuli-responsive strategies for titanium implant functionalization in bone regeneration and therapeutics, Mater. Horiz. 11 (2024) 12–36.
[7] J. Zhang, C. Zhao, R. Sheng, K. Lin, X. Wang, S. Zhang, Construction of a hierarchical micro-/submicro-/nanostructured 3d-printed ti6al4v surface feature to promote osteogenesis: involvement of sema7a through the itgb1/fak/erk signaling pathway, ACS Appl. Mater. Interfaces 14 (2022) 30571–30581.
[8] M.U. Joshi, S.P. Kulkarni, M. Choppadandi, M. Keerthana, G. Kapusetti, Current state of art smart coatings for orthopedic implants: a comprehensive review, Smart Materials in Medicine 4 (2023) 661–679.
[9] K. Tang, M.L. Luo, W. Zhou, L.N. Niu, J.H. Chen, F. Wang, The integration of peri-implant soft tissues around zirconia abutments: challenges and strategies, Bioact. Mater. 27 (2023) 348–361.
[10] J.C. Kim, M. Lee, I.L. Yeo, Three interfaces of the dental implant system and their clinical effects on hard and soft tissues, Mater. Horiz. 9 (2022) 1387–1411.
[11] S. Chen, Z. Huang, R.M. Visalakshan, H. Liu, A. Bachhuka, Y. Wu, P. Dabare, P. Luo, R. Liu, Z. Gong, Y. Xiao, K. Vasilev, Z. Chen, Z. Chen, Plasma polymerized bio-interface directs fibronectin adsorption and functionalization to enhance "epithelial barrier structure" formation via fn-itg beta1-fak-mtor signaling cascade, Biomater. Res. 26 (2022) 88.
[12] N. Tatarakis, J. Bashutski, H.L. Wang, T.J. Oh, Early implant bone loss: preventable or inevitable? Implant Dent. 21 (2012) 379–386.
[13] T. Wach, M. Skorupska, G. Trybek, Are torque-induced bone texture alterations related to early marginal jawbone loss? J. Clin. Med. 11 (2022).
[14] S. Ivanovski, P.M. Bartold, Y.S. Huang, The role of foreign body response in peri-implantitis: what is the evidence? Periodontology 90 (2000 2022) 176–185.
[15] Xingchen Liu, Shudan Deng, Xiyan Li, Haiwen Liu, Zhixin Li, You Wu, Pu Luo, Xinyi Zhong, Ruoxuan Huang, Runheng Liu, et al., A standardized rat model to

study peri-implantitis of transmucosal osseointegrated implants, Biomater. Res. 28 (2024), https://doi.org/10.34133/bmr.0021.
[16] M. Usui, T. Sato, G. Yamamoto, Y. Okamatsu, T. Hanatani, Y. Moritani, K. Sano, M. Yamamoto, K. Nakashima, Gingival epithelial cells support osteoclastogenesis by producing receptor activator of nuclear factor kappa b ligand via protein kinase a signaling, J. Periodontal. Res. 51 (2016) 462–470.
[17] T. Nagasawa, H. Kobayashi, M. Kiji, M. Aramaki, R. Mahanonda, T. Kojima, Y. Murakami, M. Saito, Y. Morotome, I. Ishikawa, Lps-stimulated human gingival fibroblasts inhibit the differentiation of monocytes into osteoclasts through the production of osteoprotegerin, Clin. Exp. Immunol. 130 (2002) 338–344.
[18] Y. Chang, B. Cho, S. Kim, J. Kim, Direct conversion of fibroblasts to osteoblasts as a novel strategy for bone regeneration in elderly individuals, Exp. Mol. Med. 51 (2019) 1–8.
[19] R. Liu, S. Chen, P. Huang, G. Liu, P. Luo, Z. Li, Y. Xiao, Z. Chen, Z. Chen, Immunomodulation-based strategy for improving soft tissue and metal implant integration and its implications in the development of metal soft tissue materials, Adv. Funct. Mater. 30 (2020).
[20] W.R. Wang, J. Li, J.T. Gu, B.W. Hu, W. Qin, Y.N. Zhu, Z.X. Guo, Y.X. Ma, F. Tay, K. Jiao, L. Niu, Optimization of lactoferrin-derived amyloid coating for enhancing soft tissue seal and antibacterial activity of titanium implants, Adv. Healthcare Mater. 12 (2023) e2203086.
[21] Q. Zhao, X. Du, Multi-scale adaptions of dynamic bio-interfaces, Smart Materials in Medicine 3 (2022) 37–40.
[22] D. Palombo, M. Rahmati, F. Vignoletti, J. Sanz-Esporrin, H.J. Haugen, M. Sanz, Hard and soft tissue healing around implants with a modified implant neck configuration: an experimental *in vivo* preclinical investigation, Clin. Oral Implants Res. 32 (2021) 1127–1141.
[23] S. Chen, J. Shi, G. Gao, L. Xie, Y. Zhang, Z. Shan, Z. Huang, X. Zhang, Z. Chen, Z. Chen, Immunomodulation-based development engineering for advancing metal soft tissue implants, Smart Materials in Medicine 4 (2023) 562–577.
[24] M. Kharaziha, A. Baidya, N. Annabi, Rational design of immunomodulatory hydrogels for chronic wound healing, Adv. Mater. 33 (2021) e2100176.
[25] F. Bian, Y.W. Lan, S. Zhao, Z. Deng, S. Shukla, A. Acharya, J. Donovan, T. Le, D. Milewski, M. Bacchetta, A.E. Hozain, Y. Tipograf, Y.W. Chen, Y. Xu, D. Shi, V. V. Kalinichenko, T.V. Kalin, Lung endothelial cells regulate pulmonary fibrosis through foxf1/r-ras signaling, Nat. Commun. 14 (2023) 2560.
[26] V. Fischer, M. Haffner-Luntzer, Interaction between bone and immune cells: implications for postmenopausal osteoporosis, Semin. Cell Dev. Biol. 123 (2022) 14–21.
[27] K. Jiao, L.N. Niu, Q.H. Li, F.M. Chen, W. Zhao, J.J. Li, J.H. Chen, C.W. Cutler, D. H. Pashley, F.R. Tay, Biphasic silica/apatite co-mineralized collagen scaffolds stimulate osteogenesis and inhibit rankl-mediated osteoclastogenesis, Acta Biomater. 19 (2015) 23–32.
[28] C. Lei, J.H. Song, S. Li, Y.N. Zhu, M.Y. Liu, M.C. Wan, Z. Mu, F.R. Tay, L.N. Niu, Advances in materials-based therapeutic strategies against osteoporosis, Biomaterials 296 (2023) 122066.
[29] Z. Chen, T. Klein, R.Z. Murray, R. Crawford, J. Chang, C. Wu, Y. Xiao, Osteoimmunomodulation for the development of advanced bone biomaterials, Mater. Today 19 (2016) 304–321.
[30] Z. Yang, M. Liu, Y. Yang, M. Zheng, Y. Yang, X. Liu, J. Tan, Biofunctionalization of zirconia with cell-adhesion peptides via polydopamine crosslinking for soft tissue engineering: effects on the biological behaviors of human gingival fibroblasts and oral bacteria, RSC Adv. 10 (2020) 6200–6212.
[31] P. Huang, J. Xu, L. Xie, G. Gao, S. Chen, Z. Gong, X. Lao, Z. Shan, J. Shi, Z. Zhou, Z. Chen, Y. Cao, Y. Wang, Z. Chen, Improving hard metal implant and soft tissue integration by modulating the "inflammatory-fibrous complex" response, Bioact. Mater. 20 (2023) 42–52.
[32] D.W. Williams, T. Greenwell-Wild, L. Brenchley, N. Dutzan, A. Overmiller, A. P. Sawaya, S. Webb, D. Martin, G. Hajishengallis, K. Divaris, M. Morasso, M. Haniffa, N.M. Moutsopoulos, Human oral mucosa cell atlas reveals a stromal-neutrophil axis regulating tissue immunity, Cell 184 (2021) 4090–4104.
[33] T. Berglundh, N.U. Zitzmann, M. Donati, Are peri-implantitis lesions different from periodontitis lesions? J. Clin. Periodontol. 38 (Suppl 11) (2011) 188–202.
[34] L.C. Shanley, O.R. Mahon, D.J. Kelly, A. Dunne, Harnessing the innate and adaptive immune system for tissue repair and regeneration: considering more than macrophages, Acta Biomater. 133 (2021) 208–221.
[35] N. Su, C. Villicana, D. Barati, P. Freeman, Y. Luo, F. Yang, Stem cell membrane-coated microribbon scaffolds induce regenerative innate and adaptive immune responses in a critical-size cranial bone defect model, Adv. Mater. 35 (2023) e2208781.
[36] B. Chen, W. Wu, W. Sun, Q. Zhang, F. Yan, Y. Xiao, Rankl expression in periodontal disease: where does rankl come from? BioMed Res. Int. 2014 (2014) 731039.
[37] M. Usui, S. Onizuka, T. Sato, S. Kokabu, W. Ariyoshi, K. Nakashima, Mechanism of alveolar bone destruction in periodontitis - periodontal bacteria and inflammation, Japanese Dental Science Review 57 (2021) 201–208.
[38] M.J. Shen, C.Y. Wang, D.X. Hao, J.X. Hao, Y.F. Zhu, X.X. Han, L. Tonggu, J. H. Chen, K. Jiao, F.R. Tay, L.N. Niu, Multifunctional nanomachinery for enhancement of bone healing, Adv. Mater. 34 (2022) e2107924.
[39] J. Li, J.F. Yan, Q.Q. Wan, M.J. Shen, Y.X. Ma, J.T. Gu, P. Gao, X.Y. Tang, F. Yu, J. H. Chen, F.R. Tay, K. Jiao, L.N. Niu, Matrix stiffening by self-mineralizable guided bone regeneration, Acta Biomater. 125 (2021) 112–125.
[40] N. Wada, H. Maeda, Y. Yoshimine, A. Akamine, Lipopolysaccharide stimulates expression of osteoprotegerin and receptor activator of nf-kappa b ligand in periodontal ligament fibroblasts through the induction of interleukin-1 beta and tumor necrosis factor-alpha, Bone 35 (2004) 629–635.
[41] M.I. Koehler, E.S. Hartmann, S. Schluessel, F. Beck, J.I. Redeker, B. Schmitt, M. Unger, M. van Griensven, B. Summer, A. Fottner, Mayer-Wagner S: impact of periprosthetic fibroblast-like cells on osteoclastogenesis in co-culture with peripheral blood mononuclear cells varies depending on culture system, Int. J. Mol. Sci. 20 (2019).
[42] A. Chaparro, V. Beltran, D. Betancur, Y.H. Sam, H. Moaven, A. Tarjomani, N. Donos, V. Sousa, Molecular biomarkers in peri-implant health and disease: a cross-sectional pilot study, Int. J. Mol. Sci. 23 (2022).
[43] T. Albrektsson, C. Dahlin, D. Reinedahl, P. Tengvall, R. Trindade, A. Wennerberg, An imbalance of the immune system instead of a disease behind marginal bone loss around oral implants: position paper, Int. J. Oral Maxillofac. Implants 35 (2020) 495–502.
[44] W.R. Wang, J. Li, J.T. Gu, B.W. Hu, W. Qin, Y.N. Zhu, Z.X. Guo, Y.X. Ma, F. Tay, K. Jiao, L. Niu, Optimization of lactoferrin-derived amyloid coating for enhancing soft tissue seal and antibacterial activity of Titanium Implants, Adv. Healthcare Mat. 12 (11) (2023) e2203086, https://doi.org/10.1002/adhm.202203086.
[45] Y. Li, J. Zhang, W. Cai, C. Wang, Z. Yu, Z. Jiang, K. Lai, Y. Wang, G. Yang, Creb3l2 regulates hemidesmosome formation during epithelial sealing, J. Dent. Res. 102 (2023) 1199–1209.
[46] N. Jacob, K. Kumagai, J.P. Abraham, Y. Shimodaira, Y. Ye, J. Luu, A.Y. Blackwood, S.L. Castanon, D.T. Stamps, L.S. Thomas, R. Gonsky, D.Q. Shih, K.S. Michelsen, S. R. Targan, Direct signaling of tl1a-dr3 on fibroblasts induces intestinal fibrosis *in vivo*, Sci. Rep. 10 (2020) 18189.
[47] O.J. Culley, B. Louis, C. Philippeos, B. Oules, M. Tihy, J.M. Segal, D. Hyliands, G. Jenkins, R.K. Bhogal, R.C. Siow, F.M. Watt, Differential expression of insulin-like growth factor 1 and wnt family member 4 correlates with functional heterogeneity of human dermal fibroblasts, Front. Cell Dev. Biol. 9 (2021) 628039.